Experimental evidence for topological surface states wrapping around a bulk SnTe crystal

K. Dybko,* M. Szot, A. Szczerbakow, M. U. Gutowska, T. Zajarniuk, J. Z. Domagala, A. Szewczyk, T. Story, and W. Zawadzki
Institute of Physics, Polish Academy of Sciences, Aleja Lotnikow 32/46, PL-02668 Warsaw, Poland
(Received 13 July 2017; published 15 November 2017)

We demonstrate that the metallic topological surface states *wrap on all sides* the three-dimensional topological crystalline insulator SnTe. This is achieved by studying oscillatory quantum magnetotransport and magnetization at tilted magnetic fields, which enables us to observe simultaneous contributions from neighboring sample sides. Taking into account pinning of the Fermi energy by the SnTe reservoir, we successfully describe theoretically the de Haas–van Alphen oscillations of magnetization. The determined π–Berry phase of surface states confirms their Dirac fermion character. We independently observe oscillatory contributions of magnetotransport and magnetization originating from the bulk SnTe reservoir of high hole density. It is concluded that the bulk and surface Landau states exist in parallel. Our main result that the bulk reservoir is surrounded on all sides by the topological surface states has a universal character.

DOI: 10.1103/PhysRevB.96.205129

I. INTRODUCTION

Topological insulators (TIs) and topological crystalline insulators (TCIs) are new phases of quantum matter with topologically protected gapless boundary states. The topological protection is ensured by time-reversal symmetry (TIs) or specific crystalline symmetry (TCIs), respectively. It was predicted theoretically for a nontrivial band ordering of a bulk semiconductor that the two-dimensional (2D) topologically protected surface states appear on *all* surfaces of the bulk material [1,2]. For two opposite surfaces, this property was demonstrated experimentally for thin films of strained HgTe [3] and unstrained $BiSbTeSe_2$ [4]. A separation of the Shubnikov–de Haas oscillations originating from the two surfaces was achieved because they had different 2D electron densities [3]. The IV-VI compound SnTe, having the rock-salt crystal symmetry and the nontrivial band ordering at the L points of the Brillouin zone, is known to generate the topological states of the TCIs at the (001), (110), and (111) surfaces. This was first demonstrated in the angle-resolved photoemission spectroscopy (ARPES) studies [5,6] and by scanning tunneling spectroscopy [7,8]. Also, there has been a suggestion based on the Shubnikov–de Haas experiment that the Dirac fermions exist on the (111) surface of SnTe, grown as a thin film on a Bi_2Te_3 buffer layer [9]. The other transport studies of SnTe are limited to observations of low-field weak antilocalization of massless Dirac fermions on single surfaces of thin films oriented along (001) or (111) planes [10,11].

In the present work, we show that the topological surface states (TSSs) appear equally well on neighboring surfaces, thus wrapping the bulk SnTe sample. As compared to the strained HgTe, our system has two distinct properties. First, we deal with topological crystalline insulators whose topological protection is assured by the proper order and symmetry of energy bands in bulk SnTe; see [5,12–14]. Second, we deal with a large reservoir of holes in the bulk SnTe which pins the Fermi level of the entire system and determines the properties of TSSs. We study the quantized Hall regime, the Shubnikov–de Haas (SdH) effect, and the de Haas–van Alphen effect. In order to separate contributions of the two investigated surfaces, we rotate our sample with respect to the direction of magnetic field. In the studies of TIs, one usually tries to suppress the effect of the bulk by reducing its volume, carrier density, etc. The very high quality of our samples allows us to separate contributions of the bulk and surface states without recourse to any additional measures, so we deal with natural as-grown SnTe crystals [15].

II. EXPERIMENT

The SnTe samples were cleaved along the (100) plane and equivalent planes, as checked by the x-ray Laue diffraction. Thus the sample is surrounded on all sides by the surfaces hosting TCI states. The high crystal quality of our sample is illustrated in Fig. S1 of the Supplemental Material [16]. The Hall-bar geometry with six contacts was used in transport experiments. Figure 1(a) shows raw data of magnetoresistivity tensor components measured for $B \parallel [001]$ probing the top and bottom surfaces. The results of R_{xx} and R_{xy}, while showing slight wavy behavior due to SdH oscillations and the contribution of the quantum Hall effect, do not exhibit the usual plateaus of R_{xy} and zeros of R_{xx}. The Hall resistivity is several orders of magnitude lower than the expected kΩ range. This becomes understandable when one takes into account that the transport has two components: the surfaces and the bulk. The bulk of SnTe, having very large hole density, plays the role of a reservoir for the system. This reservoir short circuits the surface conductivity. The role of reservoir in the magnetoconductivity of 2D semiconductor systems is known; see Refs. [17–19]. In particular, it was observed, in agreement with our data, that the reservoir dramatically lowers measured values of the Hall voltage in the quantum Hall regime [20,21]. Another important effect of a large reservoir is to pin the Fermi level of the system.

To characterize the quantum behavior of our system, we subtract smooth backgrounds of the data shown in Fig. 1(a). The resulting oscillatory behavior, plotted in $1/B$ scale, is shown in the inset. The observed frequency of both R_{xy} and R_{xx} oscillations is 26 T and they are shifted with respect to each other by a constant phase factor $1/4$ of the full period 2π. This frequency corresponds to $N_s = 6.2 \times 10^{11}$ cm^{-2} of holes,

*Krzysztof.Dybko@ifpan.edu.pl

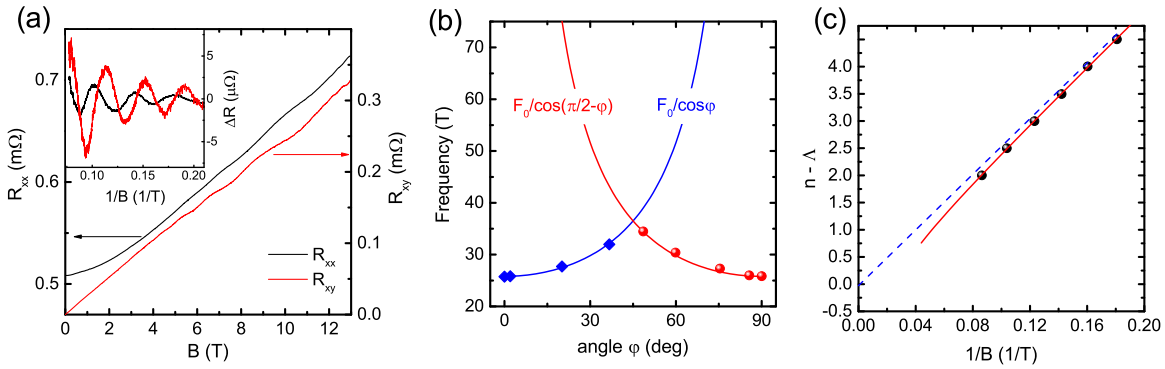

FIG. 1. The Shubnikov–de Haas and quantum Hall oscillations of topological surface states in SnTe. (a) Raw R_{xx} and R_{xy} resistances vs magnetic field taken at $\boldsymbol{B} \parallel [001]$. Wavy lines are the sums of the bulk and surface contributions. Very small values of R_{xy} are caused by the high hole density of bulk SnTe. Inset: Oscillatory components ΔR_{xx} and ΔR_{xy} obtained by subtracting smooth backgrounds. (b) Frequencies of SdH oscillations related to the topological surface states, as extracted from chirp Z-transform for different tilt angles. Blue diamonds: experiment. The blue line represents $F_0/\cos(\varphi)$ dependence related to the top and bottom surfaces. Red circles: experiment. The red line represents $F_0/\cos(\pi/2-\varphi)$ dependence for the side surfaces. (c) Landau-level index plot of R_{xx} extrema related to the surface states vs $1/B$. Nonlinear fit (see Ref. [21]) yields the Berry phase of π characteristic of the topological surface states.

according to the Lifshitz-Kosevich theory of SdH oscillations of 2D gas [22]. The observed phase factor satisfies the resistivity rule $R_{xx} \sim B \cdot dR_{xy}/dB$ commonly obeyed in the integer quantum Hall regime [23], indicating that we deal with 2D states; see Fig. S2 in the Supplemental Material [16]. It can be seen that in the high-field region of $1/B < 0.11\,\mathrm{T}^{-1}$, there appear small-amplitude oscillations better seen in B scale (see Fig. S3 in the Supplemental Material [16]). Their frequency is roughly 322 T, indicating that the oscillations originate from ellipsoids at the L points of 3D SnTe. This conclusion is additionally confirmed by the angular dependence of the observed frequencies [16]. The above analysis clearly shows that our transport results represent a sum of surface and bulk contributions.

To demonstrate that the topological surface states exist on *all* 2D boundaries of the SnTe sample, we analyze the R_{xx} resistance measured for a magnetic field tilted with respect to the [001] crystal direction. In this configuration, the magnetic field has components normal to both neighboring surfaces and thus both of them contribute to the magnetoresistance tensor. The oscillatory data were analyzed using the chirp Z-transform [24]. This generalization of the discrete Fourier transform is often applied to data obscured by considerable noise. The results of our analysis, shown in Fig. 1(b), are characterized by the following important features. First, the frequency originating from one surface follows the $F_0/\cos\varphi$ dependence. Second, one observes a contribution of the other surface following the $F_0/\cos[(\pi/2)-\varphi]$ dependence. Third, the complete symmetry of angular dependences for the two surfaces shows that the top and side surfaces are characterized by identical states. The chirp analysis did not reveal any additional frequency at $\varphi = 0^\circ$ or $\varphi = 90^\circ$, which means that the opposite surfaces are equivalent.

We also determine the Berry phase of our TSSs. In Fig. 1(c), we show the Landau-level index plot of SdH extrema versus *1/B*. According to the theory [25–27], such plots are nonlinear functions of *1/B* at high fields (or low numbers n). The Berry phase is determined by the asymptotic limit of such a plot for low fields. Figure 1(c) indicates the best fit to the data (red solid line) as well as its asymptote (dashed blue line). The determined phase offset γ is -0.03 ± 0.03. Thus, within the experimental accuracy, we obtain $\gamma \approx 0$, which corresponds to the nontrivial Berry phase of π characteristic of the Dirac fermions [26,27]. The analogous statement is also true for other tilt angles, as illustrated in Fig. S13 of the Supplemental Material [16]. These facts confirm the topological origin of the observed surface states, which wrap all the way around the TCI SnTe sample.

We independently investigate the de Haas–van Alphen (dHvA) oscillations of magnetization. The magnetization depends only on the density of states and is a simpler phenomenon than magnetotransport, with the latter being also influenced by the carriers' scattering. As in the case of transport, the magnetization is composed of bulk SnTe and TSS contributions. Our measurements were carried out on freshly cleaved rectangular SnTe samples, similar to those used in the electric transport studies. The raw magnetization data contain a smooth nonoscillatory background (see Fig. S7 of the Supplemental Material [16]). After this background is subtracted, the oscillatory component has the form shown in Fig. 2(a) for three temperatures.

To understand the observed behavior, one must account for the presence of the SnTe bulk carrier reservoir in contact with the surface states. To describe quantitatively our magnetization data, we need to know an explicit form for the Landau-level energies in TCIs. This form is well approximated for the valence band by the following formula (see [25]):

$$E_n = \sqrt{2ne\hbar B v_F^2 + (g^*\mu_B B/2)^2}, \tag{1}$$

where n is the Landau-level number, e is the elementary charge, h is the Planck constant, μ_B is the Bohr magneton, and g^* is the effective spin g factor in the standard notation. The density of states (DOS) for a 2D system in the presence of a magnetic field is

$$\rho(E) = \frac{1}{2\pi L^2} \sum_n \sqrt{\frac{2}{\pi}} \frac{1}{\Gamma} \exp\left[-2\left(\frac{E-E_n}{\Gamma}\right)^2\right], \tag{2}$$

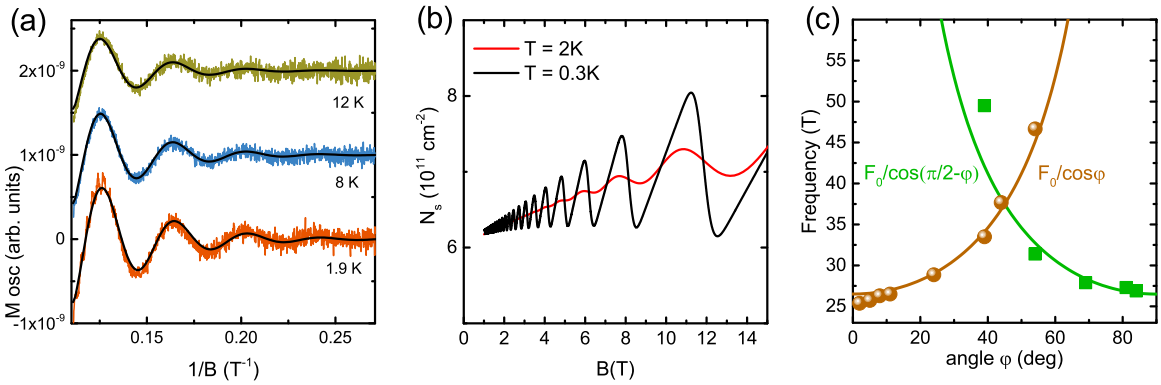

FIG. 2. Charge transfer and oscillatory magnetization of topological surface states in SnTe. (a) Oscillatory magnetization measured for the SnTe vs $1/B$ (the traces are shifted for clarity). Black solid lines are calculated for the Fermi energy pinned by the bulk reservoir using $E_F = 80$ meV, $v_F = 4.4 \times 10^5$ m/s, $\Gamma_0 = 4.5$ meV, $g* = 57$. (b) Oscillations of hole density in surface states calculated assuming that the bulk SnTe reservoir pins the Fermi energy of the system. (c) Frequencies of dHvA oscillations related to the TSSs, as extracted from chirp Z-transform for different tilt angles of magnetic field. Brown circles: experiment. The brown line represents $F_0/\cos(\varphi)$ dependence related to the top and bottom surfaces. Green squares: experiment. The green line represents $F_0/\cos(\pi/2 - \varphi)$ dependence for the side surfaces. For tilt angles 39° and 54°, simultaneous contributions of two neighboring surfaces are observed.

where E_n is given above, $L^2 = \hbar/eB$, and Γ is the broadening of Gaussian peaks. The 2D electron density is given by

$$N_s = \int_0^\infty \frac{\rho(E)}{1 + \exp\left[(E - E_F)/k_B T\right]}\, dE, \qquad (3)$$

where E_F is the Fermi energy. As the magnetic field changes, the holes from the bulk SnTe reservoir go back and forth to the topological 2D surface states, as illustrated in Fig. 2(b). It is seen that changes of the hole density in TSSs at $T = 0.3$ K are around 30%. It is a sizable amount for TSSs, but a negligible one for the reservoir of bulk SnTe. In principle, the Fermi energy in the bulk varies somewhat with the magnetic field, but its changes are very slight [28]. In TSSs, we deal with a system characterized by a varying number of particles described by the grand canonical ensemble. Its potential Ω is

$$\Omega = -k_B T \int_{-\infty}^{+\infty} \rho(E) \ln\left[1 + \exp\left(\frac{E - E_F}{k_B T}\right)\right] dE. \qquad (4)$$

For semiconductor quantum wells in the presence of a quantizing magnetic field, one usually considers two cases [17]. In the first, the number of carriers is constant and the Fermi energy oscillates. In the second, the Fermi energy is fixed by a reservoir and the number of carriers oscillates. In this case, one has to take into account the fact that the electrostatic confining potential depends on the electric charge, so the system "breathes" when the carriers move back and forth [17]. Here, we deal with the third case in which the Fermi energy is fixed by the reservoir and the carriers also move back and forth, but since we do not deal with the confining potential, the system does not "breathe." In our description, we compute the grand potential Ω with the fixed value of the Fermi energy and then calculate the magnetization directly from the relation $M = -\partial\Omega/\partial B|_{E_F}$.

The calculations were carried for the parameters indicated in the caption of Fig. 2(a). From the frequency of dHvA oscillations, we determine the hole density $N_s = 6.1 \times 10^{11}$ cm^{-2}, and from the temperature dependence of their amplitudes the cyclotron effective mass $m^* = 0.08 m_0$ [16]. Using the relation between the Fermi wave vector k_F and the density for spin-polarized 2D states, $k_F = \sqrt{4\pi N_s} = 2.7 \times 10^8$ m^{-1}, one obtains the Fermi velocity $v_F = \hbar k_F/m^* = 4 \times 10^5$ m/s, which determines the linear Dirac dispersion of TSSs. The above value agrees quite well with that determined in ARPES studies of SnTe, which also demonstrates that we deal with the surface states of holes [5]. The remaining parameters Γ and g^* are adjusted to fit the dHvA oscillations. We take into account the field dependence of the level broadening, $\Gamma = \Gamma_0\sqrt{B}$ [29,30]. As to the large value of $g^* = 57$, it results from the large spin-orbit interaction already manifested in the large bulk g factors in SnTe [31,32]. Figure 2(a) shows our oscillatory dHvA experimental results for magnetic field $B\|[001]$ crystal direction and their theoretical description in the $1/B$ scale. The frequency of dHvA oscillations is around 25.4 T, corresponding to the hole density of $N_s = 6.1 \times 10^{11}$ cm^{-2}. This is in agreement with the result of the SdH oscillations obtained on a different sample ($N_s = 6.2 \times 10^{11}$ cm^{-2}). All in all, we reach a very good description of the oscillating magnetization of TSSs at various temperatures, thus confirming the charge transfer illustrated in Fig. 2(b).

Next, similar to the procedure applied to the transport effects, we tilt the magnetic field in order to investigate the magnetization of the top and side surfaces together with their parallel counterparts. Figure S9(a) shows a chirp Z-transform power spectrum for different tilt angles (see Supplemental Material [16]). Final results of our analysis are summarized in Fig. 2(c), which shows the dHvA frequencies obtained for the magnetic field tilted at different angles. These frequencies obey the same angle dependences as those followed by the SdH frequencies shown in Fig. 1(b), which confirms that we deal as before with the top and bottom surfaces, on the one hand, and two side surfaces, on the other. It is seen that for two angles, 39°and 54°, one observes two different frequencies related to neighboring surfaces. Thus, the magnetization measurements fully confirm and

augment the results described above for the transport data. In addition, as analyzed in the Supplemental Material [16], one obtains an identical π–Berry phase characteristic of the Dirac fermions.

The magnetization data shown in Fig. 2(a) exhibit for low values of *1/B* also high-frequency dHvA oscillations. They are better seen in a plot versus B; see Fig. S8 of the Supplemental Material [16]. Analyzing these oscillations for tilted magnetic fields, we identify them as originating from the 3D SnTe reservoir and determine the corresponding hole density to be $N_B = 1.4 \times 10^{20}\,\mathrm{cm}^{-3}$. Thus the magnetization data fully confirm also for the bulk reservoir the information obtained from magnetotransport. Thus, our data unambiguously indicate that in spite of very high hole density in bulk SnTe and overlapping energies of the bulk and surface states, there exist completely independent sets of Landau levels in both subsystems.

III. DISCUSSION

It should be noted that in early papers on SnTe [33,34], the authors observed, at hole densities above $2.2 \times 10^{20}\,\mathrm{cm}^{-3}$, magneto-oscillations at the frequency range of 30–60 T, similar to our results shown in Figs. 1(b) and 2(c). Since at that time the TSSs were unknown, the observations were attributed to a second valence band at the Σ points of the bulk Brillouin zone [31]. However, we unambiguously demonstrate above, with the use of the quantum Hall effect, the angular dependence of SdH and dHvA oscillations, and their π-Berry phase, that we observe the 2D topological surface states revealed in the ARPES studies [5]. An additional indication that the results of [33,34] should be attributed to the 2D states is that the bulk Σ band in IV-VI rock-salt materials should be manifested by *two* sets of magneto-oscillations with strongly different frequencies [35], whereas the early data and our results show only a single frequency.

Finally, one may be surprised that we observe the contributions of surface states in spite of the very large difference of hole densities between the bulk reservoir and the surface. This problem was noted by Taskin and Ando [36]. We may add that the same situation occurs also in other studies [37,38] in which a clear contribution of the surface states has been observed.

In summary, it is experimentally demonstrated that as-grown bulk SnTe is *surrounded on all sides* by the metallic 2D topological surface states. We study surface and bulk states of topological crystalline insulator SnTe by investigating quantum magnetotransport and magnetization. Bulk and surface components are separated using the oscillatory character of the studied effects. By tilting the external magnetic field, we establish contributions of the topological states originating from neighboring surfaces that are perpendicular to each other. The correlation of quantum oscillations of the Hall and longitudinal magnetoresistances is observed. The magnetization data are described theoretically, taking into account that the bulk SnTe reservoir pins the Fermi energy of the whole system. Landau-level index plots are used to determine the Berry phase of π in magnetotransport and magnetization oscillations, confirming that the identified surface states are topological Dirac fermions. In all observations, the presence of the large bulk reservoir of holes is strongly felt. The presented findings have universal character and apply to other topological crystalline insulators as well as to topological insulators.

ACKNOWLEDGMENTS

We gratefully acknowledge elucidating discussions with Prof. T. Dietl. The work has been supported in part by the Polish National Science Centre Grants No. 2012/07/B/ST3/03607 and No. 2014/15/B/ST3/03833.

[1] L. Fu, C. L. Kane, and E. J. Mele, Phys. Rev. Lett. **98**, 106803 (2007).
[2] Y. Ando and L. Fu, Annu. Rev. Condens. Matter Phys. **6**, 361 (2015).
[3] C. Bruene, C. X. Liu, E. G. Novik, E. M. Hankiewicz, H. Buhmann, Y. L. Chen, X. L. Qi, Z. X. Shen, S. C. Zhang, and L. W. Molenkamp, Phys. Rev. Lett. **106**, 126803 (2011).
[4] Y. Xu, I. Miotkowski, and Y. P. Chen, Nat. Commun. **7**, 11434 (2016).
[5] Y. Tanaka, Z. Ren, T. Sato, K. Nakayama, S. Souma, T. Takahashi, K. Segawa, and Y. Ando, Nat. Phys. **8**, 800 (2012).
[6] Y. Tanaka, T. Shoman, K. Nakayama, S. Souma, T. Sato, T. Takahashi, M. Novak, K. Segawa, and Y. Ando, Phys. Rev. B **88**, 235126 (2013).
[7] Y. Okada, M. Serbyn, H. Lin, D. Walkup, W. Zhou, C. Dhital, M. Neupane, S. Xu, Y. J. Wang, R. Sankar, F. Chou, A. Bansil, M. Z. Hasan, S. D. Wilson, L. Fu, and V. Madhavan, Science **341**, 1496 (2013).
[8] P. Sessi, D. Di Sante, A. Szczerbakow, F. Glott, S. Wilfert, H. Schmidt, T. Bathon, P. Dziawa, M. Greiter, T. Neupert, G. Sangiovanni, T. Story, R. Thomale, and M. Bode, Science **354**, 1269 (2016).
[9] A. A. Taskin, F. Yang, S. Sasaki, K. Segawa, and Y. Ando, Phys. Rev. B **89**, 121302 (2014).
[10] B. A. Assaf, F. Katmis, P. Wei, B. Satpati, Z. Zhang, S. P. Bennett, V. G. Harris, J. S. Moodera, and D. Heiman, Appl. Phys. Lett. **105**, 102108 (2014).
[11] R. Akiyama, K. Fujisawa, T. Yamaguchi, R. Ishikawa, and S. Kuroda, Nano Res. **9**, 490 (2016).
[12] T. H. Hsieh, H. Lin, J. Liu, W. Duan, A. Bansil, and L. Fu, Nat. Commun. **3**, 982 (2012).
[13] P. Dziawa, B. J. Kowalski, K. Dybko, R. Buczko, A. Szczerbakow, M. Szot, E. Łusakowska, T. Balasubramanian, B. M. Wojek, M. H. Berntsen, O. Tjernberg, and T. Story, Nat. Mater. **11**, 1023 (2012).
[14] S.-Y. Xu, C. Liu, N. Alidoust, M. Neupane, D. Qian, I. Belopolski, J. D. Denlinger, Y. J. Wang, H. Lin, L. A. Wray, G. Landolt, B. Slomski, J. H. Dil, A. Marcinkova, E. Morosan, Q. Gibson, R. Sankar, F. C. Chou, R. J. Cava, A. Bansil, and M. Z. Hasan, Nat. Commun. **3**, 1192 (2012).

[15] A. Szczerbakow and K. Durose, Prog. Cryst. Growth Charact. Mater. **51**, 81 (2005).
[16] See Supplemental Material at http://link.aps.org/supplemental/10.1103/PhysRevB.96.205129 doi for additional experimental and technical details, including Refs. [39–42].
[17] W. Zawadzki, A. Raymond, and M. Kubisa, Phys. Status Solidi **251**, 247 (2014).
[18] M. Von Ortenberg, O. Portugall, W. Dobrowolski, A. Mycielski, R. R. Galazka, and F. Herlach, J. Phys. C Solid State Phys. **21**, 5393 (1988).
[19] J. G. Analytis, R. D. McDonald, S. C. Riggs, J.-H. Chu, G. S. Boebinger, and I. R. Fisher, Nat. Phys. **6**, 960 (2010).
[20] M. Sasaki, N. Miyajima, H. Negishi, M. Inoue, V. A. Kulbachinskii, K. Suga, Y. Narumi, and K. Kindo, Phys. B **298**, 510 (2001).
[21] N. Miyajima, M. Sasaki, H. Negishi, M. Inoue, V. A. Kulbachinskii, A. Y. Kaminskii, and K. Suga, J. Low Temp. Phys. **123**, 219 (2001).
[22] D. Shoenberg, *Magnetic Oscillations in Metals* (Cambridge University Press, Cambridge, 1984).
[23] S. H. Simon and B. I. Halperin, Phys. Rev. Lett. **73**, 3278 (1994).
[24] L. Rabiner, R. Schafer, and C. Rader, IEEE Trans. Audio Electroacoust. **17**, 86 (1969).
[25] Z. Wang, Z.-G. Fu, S.-X. Wang, and P. Zhang, Phys. Rev. B **82**, 085429 (2010).
[26] G. P. Mikitik and Y. V. Sharlai, Phys. Rev. B **85**, 033301 (2012).
[27] A. R. Wright and R. H. McKenzie, Phys. Rev. B **87**, 085411 (2013).
[28] J. S. Blakemore, *Semiconductor Statistics* (Pergamon, New York, 1962).
[29] T. Ando and Y. Uemura, J. Phys. Soc. Jpn. **36**, 959 (1974).
[30] J. P. Eisenstein, H. L. Stormer, V. Narayanamurti, A. Y. Cho, A. C. Gossard, and C. W. Tu, Phys. Rev. Lett. **55**, 875 (1985).
[31] R. L. Bernick and L. Kleinman, Solid State Commun. **8**, 569 (1970).
[32] O. Pankratov and B. Volkow, in *Physics Reviews*, edited by I. Khalatnikov (Harwood Academic, Switzerland, 1987), pp. 357–446.
[33] J. R. Burke, R. S. Allgaier, B. B. Houston, J. Babiskin, and P. G. Siebenmann, Phys. Rev. Lett. **14**, 360 (1965).
[34] H. T. Savage, B. Houston, and J. R. Burke, Phys. Rev. B **6**, 2292 (1972).
[35] P. Giraldo-Gallo, B. Sangiorgio, P. Walmsley, H. J. Silverstein, M. Fechner, S. C. Riggs, T. H. Geballe, N. A. Spaldin, and I. R. Fisher, Phys. Rev. B **94**, 195141 (2016).
[36] A. A. Taskin and Y. Ando, Phys. Rev. B **80**, 085303 (2009).
[37] M. Petrushevsky, E. Lahoud, A. Ron, E. Maniv, I. Diamant, I. Neder, S. Wiedmann, V. K. Guduru, F. Chiappini, U. Zeitler, J. C. Maan, K. Chashka, A. Kanigel, and Y. Dagan, Phys. Rev. B **86**, 045131 (2012).
[38] Z. Zhang, W. Wei, F. Yang, Z. Zhu, M. Guo, Y. Feng, D. Yu, M. Yao, N. Harrison, R. McDonald, Y. Zhang, D. Guan, D. Qian, J. Jia, and Y. Wang, Phys. Rev. B **92**, 235402 (2015).
[39] G. Springholz and G. Bauer, *Semiconductors, IV-VI*, Wiley Encycl. Electr. Electron. Eng. (Wiley, New York, 2014), pp. 1–16.
[40] J. Xiong, Y. Luo, Y. Khoo, S. Jia, R. J. Cava, and N. P. Ong, Phys. Rev. B **86**, 045314 (2012).
[41] T. Ando, A. B. Fowler, and F. Stern, Rev. Mod. Phys. **54**, 437 (1982).
[42] G. Nachtwei, D. Schulze, G. Gobsch, G. Paasch, W. Kraak, H. Krüger, and R. Herrmann, Phys. Status Solidi **148**, 349 (1988).